

# Dynamic Contour Error Estimation and Feedback Modification for High-Precision Contouring

Azad Ghaffari, *Member, IEEE*, and A. Galip Ulsoy, *Fellow, IEEE*

**Abstract**—Cross-coupling control (CCC), which acts on contour error, is intended to improve contouring precision of multi-axis servosystems. The contour error estimate (CEE) significantly affects contouring precision. Conventional CEE methods rely on static single-point techniques to reconstruct contour error using current position error and an estimate of the reference map at the lead point. The performance of such static CEE methods deteriorates dramatically with increasing contour feedrate and at sharp corners. Hence, a dynamic CEE algorithm based on the Newton update algorithm is proposed to achieve high-precision CEE. Since the convergence rate of the Newton algorithm is user assignable and independent of the reference contour, the proposed CEE stays almost identical to the contour error for vastly different feedrates or sharp corners. Multi-axis cross-coupling adds more design steps for the position control loops. Therefore, in this paper, feedback signals are modified such that a separate cross-coupling controller is no longer needed. It has been shown, analytically and experimentally, that the modified feedback in combination with integral sliding mode control (ISMC) provides simpler design and fewer steps in comparison to conventional CCC designs. Moreover, the proposed CEE and the concept of modified feedback together result in reduced contour error. Various experiments are reported to show the effectiveness of the proposed algorithm at high feedrates and for sharp corners.

**Index Terms**—Servosystems, estimation, iterative algorithms, Newton method, sliding mode control.

## I. INTRODUCTION

THE contour error (see Fig. 1(a)) in multidimensional contouring is defined as the shortest distance between the actual position and the reference contour. High-performance position control algorithms are important for reducing contour error [8], [14]. However, position control algorithms usually are designed for a specific servosystem to track a basic group of reference maps. Moreover, in reality it is not practical to develop a controller to cover a wide range of reference maps with vastly different feedrates and curvatures. Regardless of the system's dynamic accuracy and advanced control design, all position control algorithms act in the tangential direction with respect to the reference maps while the contour error is measured in the normal direction from the current position to the reference map. In response to this contouring problem, Koren [15], [16] proposed the idea of the cross-coupling control (CCC) for linear and circular contours which was then further developed and enhanced in subsequent research [2]–[4], [12], [13], [17], [20], [23], [24], [27]. Recently, Tang and Landers [28] have presented a comparative survey on published cross-coupling algorithms up to 2012.

The CCC algorithm differs from position synchronization algorithms which are used when a number of servosystems (or other moving structures) are required to follow the same tasks simultaneously [18], [26], [30]. More specifically, cross-coupling control algorithms reduce the contour error in a standalone servosystem, such as a machine tool, while position synchronization algorithms maintain the same level of position precision among a group of servosystems or parallel axes. A high-precision position synchronization algorithm may not guarantee high-precision contouring or vice versa.

To understand the need for, and effect of, the CCC algorithm in high precision contouring one needs to distinguish between the objectives of position tracking and contouring. The objective of position tracking is reaching the target point without specific requirements on the path to the target point. It is always possible to design the position control such that certain transient performance features, like response time and steady state error, are satisfied. However, in contouring, staying as close as possible to the reference map is as important as tracking the lead point of the reference map. In other words, the position control governs the contour to the current reference without considering the past reference data. The contouring process can be divided into two phases: 1) tracking phase and 2) reaching phase. The position control is usually designed to achieve the tracking phase while the CCC algorithm guarantees that the contour reaches to the closest vicinity of the reference map. Geometrically, the position control acts in the tangential direction with respect to the current reference point and the CCC acts in the normal direction. Summation of the control signals issued by the position controller and the CCC guarantees reduced contour error in comparison to the case without CCC. When model uncertainties and external disturbances are present the effect of the CCC algorithm is more pronounced.

Obtaining a close estimate of the contour error is crucial prior to CCC design. The Contour Error Estimate (CEE) is a key part of each CCC algorithm [6], [15], [19], [25], [31]–[33], [35]. Current CEE algorithms rely on algebraic methods which use the reference map information and actual position and velocity in order to calculate the estimate of the contour error in a single step. However, such static CEE algorithms are not sufficiently accurate for high feedrate reference signals or for contour maps with sharp corners and deep curves.

A static CEE uses linear or circular approximation of the contour at each time step in order to provide an estimation of the contour error. The static CEE methods are based upon the Taylor series expansion with different levels of precision. Thus, when the current position error suddenly increases or

Authors are with Department of Mechanical Engineering, University of Michigan, Ann Arbor, MI 48109-2125, aghaffar@umich.edu and ulsoy@umich.edu.

when the reference contour is highly-curved, then the reliability of the static CEE algorithm deteriorates dramatically. A dynamic CEE algorithm is presented here to overcome the limitations imposed by static CEE algorithms.

Assume that the contour map is smooth and the current position is located close to the reference contour. One can then approximate the distance between the current position and the reference contour as a quadratic function with a local minimum point associated with the contour error and use an extremum seeking algorithm to find the location and value of the contour error. Gradient-descent algorithms find the local extremum point using the actual or estimated value of the cost function gradient. However, gradient-descent depends on the cost function shape. The contour error in a Computer Numerically Controlled (CNC) system generates a wide range of cost functions with vastly different curvature which changes from one time step to the next. Newton-based extremum seeking is more sophisticated and removes the closed-loop performance dependence on the cost function shape [11], [21]. In this paper a dynamic CEE using the Newton-based update law is presented to achieve high-precision contouring for high-speed operation with highly-curved contour maps. Since the reference contour is known, analytically or numerically, one can reconstruct the gradient and the Hessian of the contour error at each time step [10].

The proposed CEE algorithm is multivariable by its nature and can be easily applied to multi-axis contouring structures without further modification. In order to implement the Newton-based CEE algorithm one needs to have access to the first order derivative of the reference vector. We introduce an estimate of the Hessian of the contour error using only the first order derivative of the reference vector. The proposed Hessian estimate reduces the numerical effort of the CEE algorithm and improves its convergence time.

The sliding mode class of controllers are well-known for their ability in compensating for the effect of dynamic uncertainty and external disturbances. In this paper, an integral sliding mode control (ISMC) is used for position control of each axis [18], [22], [26], [30]. Instead of designing a separate controller for cross-coupling, the concept of modified feedback is introduced to incorporate the effect of contour error in the ISMC. This modification is enabled by obtaining the components of the contour error vector in the direction of each axis. The modification reduces the control design steps, and when used with the proposed CEE, maintains accurate contouring for vastly different contour maps. A stability analysis shows that the position error and contour error asymptotically converge to zero. Moreover, the integrated control algorithm is supplied with adaptive disturbance estimation in order to enhance closed-loop performance. The effectiveness of the proposed contouring scheme is verified by conducting various experiments with reference maps with different feedrates and curvature. The experimental results confirm that the proposed algorithm performs as much as two times better than the conventional variable gain CCC. Moreover, the proposed algorithm accurately tracks contours with sharp corners.

The remainder of the paper is organized as follows. Section II presents the proposed CEE algorithms. Section III

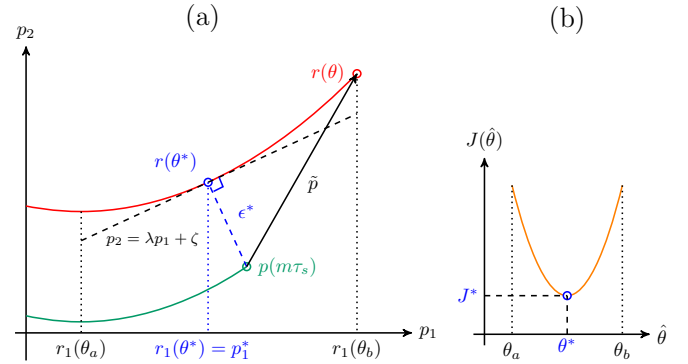


Fig. 1. (a) Contour error (b) cost function map

explains the modified feedback, ISMC design, and adaptive disturbance estimation. Section IV describes technical details of the experimental setup. Section V provides various experimental results. The last section includes the concluding remarks.

## II. NEWTON-BASED CONTOUR ERROR ESTIMATE

Dynamic equations of axis  $i$  are given as

$$\frac{d}{dt}p_i = v_i \quad (1)$$

$$\frac{d}{dt}v_i = -\frac{1}{\tau_i}v_i + \frac{k_i}{\tau_i}u_i + \frac{k_i}{\tau_i}d_i, \quad (2)$$

where  $u_i$  is command,  $d_i$  is disturbance input including load,  $v_i$  is velocity,  $p_i$  is position,  $k_i$  is DC gain, and  $\tau_i$  is time constant for axis  $i$ , where  $i = 1, 2, \dots, n$ . Position vector of the servosystem is defined as  $p(t) = [p_1(t) \ p_2(t) \ \dots \ p_n(t)]^T$ .

Assume the reference contour map is parametrized by  $\theta$

$$r(\theta) = [r_1(\theta) \ r_2(\theta) \ \dots \ r_n(\theta)]^T, \quad (3)$$

where  $\theta$  is a real number and indicates the current position along the reference path. Current position is  $p(m\tau_s)$ , where  $\tau_s$  is the sampling period of the CNC and  $m$  is the time-step number. The contour error,  $\epsilon^*$ , is the shortest distance from the current position to the reference contour. Let  $\epsilon^*$  occur at  $\theta^*$ , i.e.,  $\epsilon^* = r(\theta^*) - p(m\tau_s)$ . Denote by  $\hat{\theta}$  the estimate of  $\theta^*$ . Define a cost function as

$$J(\hat{\theta}) = \frac{1}{2} \|\epsilon(\hat{\theta})\|^2, \quad \epsilon(\hat{\theta}) = r(\hat{\theta}) - p(m\tau_s), \quad (4)$$

where  $\|\cdot\|$  represents the Euclidean norm and  $\epsilon$  is distance from current position to the reference contour. The minimum value of the cost function is associated with the values  $\epsilon^*$  and  $\theta^*$  that minimize  $J(\hat{\theta})$ . A schematic of the contour error for a two-axis system is illustrated in Fig. 1.

*Remark 1:* Assume that the current position is sufficiently close to the reference map and  $r(\theta)$  has smooth curvature everywhere. Then, at each time step, one can replace the contour with its tangent estimate,  $p_2 = \lambda p_1 + \zeta$ , where  $\lambda$  and  $\zeta$  are unknown constant parameters varying from one time step to the next. For the  $p_1 - p_2$  planar contour shown in Fig. 1, the quadratic approximate of the cost function is given as

$$J \approx J^* + \frac{1}{2}(1 + \lambda)^2 (p_1 - p_1^*)^2 \quad (5)$$

with a minimum value of

$$J^* = \left( \frac{p_2(m\tau_s) - \lambda p_1(m\tau_s) - \zeta}{\lambda^2 + 1} \right)^2 \quad (6)$$

at

$$p_1^* = \frac{p_1(m\tau_s) + (p_2(m\tau_s) - \zeta) \lambda}{\lambda^2 + 1}. \quad (7)$$

Since  $r_1(\theta^*) = p_1^*$ , one can find  $\theta^*$  from  $p_1^*$ .

Since the tangent estimate of the contour at each time step requires prior knowledge of the optimal parameter,  $\theta^*$ , the explicit approximation given by (6) and (7) cannot be implemented. Static CEE algorithms use the actual position and velocity measurements and reference contour information to approximate the tangent line in order to calculate the contour error from (6) and (7) [5], [7], [15], [19], [33], [34]. However, for high feedrates or highly curved contouring applications static CEE algorithms do not yield precise contour error estimation.

Here a dynamic CEE is proposed to estimate  $\theta^*$  and  $J^*$  in order to increase both contouring precision and speed. A plot of the cost function,  $J(\hat{\theta})$ , for a sufficiently smooth contour at time step  $m$  is shown in Fig. 1(b). The contour reference map and position measurements are available from all axes. Hence, a model-based extremum seeking algorithm, e.g., gradient-descent or the Newton-based algorithm, can be used to find  $J^*$ . Moreover, the Newton-based algorithm alleviates convergence dependence on contour shape and maintains a uniform transient over a wide range of contour shapes and feedrates. Hence, here the Newton-based extremum seeking algorithm is used [11]:

$$\frac{d}{dt} \hat{\theta} = -\alpha \frac{g}{h}, \quad (8)$$

where  $\alpha$  is a positive gain,  $g$  is the gradient and  $h$  is the Hessian of the cost function with respect to  $\hat{\theta}$ . The Newton-based CEE at each time step finds the estimate of  $\theta^*$  and  $J^*$ . One can calculate from (4) the associated contour error using  $\hat{\theta} \approx \theta^*$ .

The Newton-based algorithm requires calculation of the gradient and the Hessian. It is possible to calculate the gradient of  $J(\hat{\theta})$ , analytically or numerically

$$\begin{aligned} g &= \frac{\partial}{\partial \hat{\theta}} J(\hat{\theta}) \\ &= \epsilon^T \frac{\partial}{\partial \hat{\theta}} r(\hat{\theta}). \end{aligned} \quad (9)$$

Also, the second order derivative of  $J(\hat{\theta})$  with respect to  $\theta$ , the Hessian, is calculated as

$$\begin{aligned} h &= \frac{\partial^2}{\partial \hat{\theta}^2} J(\hat{\theta}) \\ &= \epsilon^T \frac{\partial^2}{\partial \hat{\theta}^2} r(\hat{\theta}) + \left\| \frac{\partial}{\partial \hat{\theta}} r(\hat{\theta}) \right\|^2. \end{aligned} \quad (10)$$

Assume that the contour error estimate,  $\epsilon$ , is reasonably small and the contour map has smooth curves, then one can approximate (10) as

$$h \approx \left\| \frac{\partial}{\partial \hat{\theta}} r(\hat{\theta}) \right\|^2 \quad (11)$$

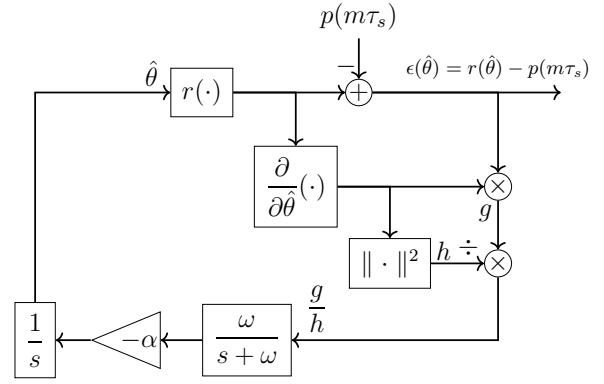


Fig. 2. Proposed Newton-based CEE

which is always positive semi-definite and improves the stability margin of the Newton-based CEE. Moreover, the computational burden for (11) is less than (10).

A schematic of the proposed Newton-based CEE is shown in Fig. 2. A linear filter is introduced to remove undesired high frequency oscillations from the parameter update law to achieve smooth transients. The filter bandwidth,  $\omega$ , is designed with respect to the control loop sampling time,  $\tau_s$ , and reference contour feedrate. Large values of  $\omega$  reduce the stability margin of the Newton-based CEE algorithm. The adaptation gain,  $\alpha$ , needs to be designed such that the Newton-based CEE is sufficiently faster than the highest reference feedrate.

*Remark 2:* The estimate of  $\theta^*$  is defined as  $\hat{\theta}$ . Denote  $\tilde{\theta} = \hat{\theta} - \theta^*$  as the parameter error. Without loss of generality and for simplicity assume  $p_1 = r_1(\hat{\theta})$ , where its linear approximation can be written as  $p_1 = p_1^* + \eta \tilde{\theta} + \mathcal{O}(\tilde{\theta}^2)$ , where  $\mathcal{O}(\cdot)$  stands for order of the terms. Replacing  $p_1$  in (5) and truncating the higher order terms gives

$$J(\tilde{\theta}) \approx J^* + \frac{1}{2} \eta^2 (1 + \lambda^2) \tilde{\theta}^2. \quad (12)$$

From the approximate cost function (12) the gradient equals  $g = \eta^2 (1 + \lambda^2) \tilde{\theta}$ . Also, the second order derivative of  $J(\tilde{\theta})$  with respect to  $\tilde{\theta}$ , the Hessian, equals  $h = \eta^2 (1 + \lambda^2)$ . Then the Newton-based update law (8) gives

$$\frac{d}{dt} \tilde{\theta} = -\alpha \tilde{\theta} \quad (13)$$

which indicates that the convergence rate and transient performance of the proposed Newton-based CEE is determined mainly by the feedback gain,  $\alpha$ .

Expansion of the stability analysis of the Newton-based CEE algorithm to multi-axis servosystems becomes more complex. However, it is possible to investigate the stability of the algorithm intuitively. Substituting (9) and (11) into the parameter update law (8) gives

$$\frac{d}{dt} \hat{\theta} = -\alpha \frac{\epsilon^T(\hat{\theta}) r_t(\hat{\theta})}{\left\| \frac{\partial}{\partial \hat{\theta}} r(\hat{\theta}) \right\|^2}, \quad r_t(\hat{\theta}) = \left( \frac{\frac{\partial}{\partial \hat{\theta}} r(\hat{\theta})}{\left\| \frac{\partial}{\partial \hat{\theta}} r(\hat{\theta}) \right\|} \right), \quad (14)$$

where  $r_t(\hat{\theta})$  is the unit tangent vector of the contour map at  $\hat{\theta}$ . Inner product of  $\epsilon$  and  $r_t$  equals  $\epsilon^T r_t$  which indicates

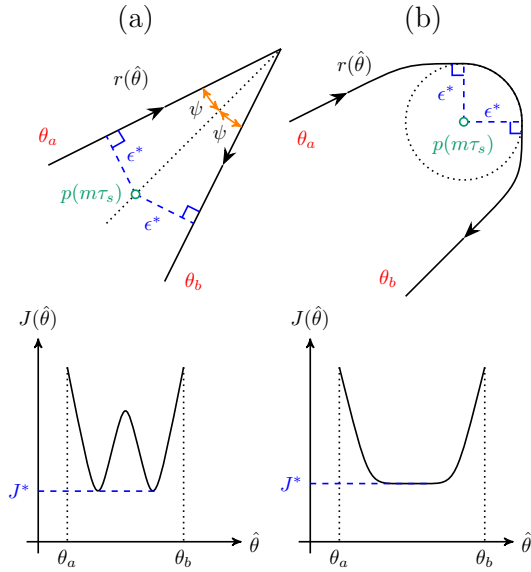


Fig. 3. Cost function with multiple extremum points for (a) sharp corners and (b) circular deep curves

the projection of contour error estimate,  $\epsilon$ , along the tangent vector. The Newton-based law (14) updates  $\hat{\theta}$  in the opposite direction of  $\epsilon^T r_t$  until  $\hat{\theta}$  reaches  $\theta^*$  where  $\epsilon^T r_t = 0$  which proves that the estimate of contour error is aligned with the contour error,  $\epsilon^*$ .

*Remark 3:* The result of the Newton-based CEE is local, meaning that one cannot guarantee global convergence. In special cases, where the reference contour has sharp corners or deep curves, as shown in Fig. 3, if the actual position is located on the dotted line at the top left-hand side contour or at the center of the dotted circle on the top right-hand side contour, the cost function will have multiple extremum points. Such cases, however, only happen at certain time steps and due to the effect of the control algorithm the next position will be off the dotted line. The same reasoning applies to the right-hand side scenario. Moreover, at each step one can initialize  $\hat{\theta}$  using the final estimate of  $\theta^*$  from the last step,  $\hat{\theta}_{m-1}$ . Without loss of generality, one can assume  $\theta$  is constantly increasing with time, then  $\hat{\theta}_{m-1}$  is close to  $\theta_a$ . Hence, the proposed Newton-based CEE converges to a local minimum closer to  $\theta_a$  which gives the actual contour error. Also, one can easily avoid these extreme scenarios by using appropriate contour interpolation.

### III. FEEDBACK MODIFICATION FOR CROSS-COUPLING

Denote position error and velocity error for each axis as  $\tilde{p}_i = r_i - p_i$  and  $\tilde{v}_i = dr_i/dt - v_i$ , respectively. The CEE vector  $\epsilon = [\epsilon_1 \ \epsilon_2 \ \dots \ \epsilon_n]^T$  is obtained from the Newton-based algorithm, where  $\epsilon_i$  indicates the effect of contour error along axis  $i$ . Existing contouring algorithms can be classified into two categories with separate controllers for: 1) position tracking and cross-coupling [15], and 2) normal and tangential directions of the contour map [20], [32]. In this work integral sliding mode control (ISMC) is used to perform position tracking along each axis. Instead of designing a separate controller for cross-coupling, the concept of modified feedback

is proposed to incorporate the effect of contour error in the system dynamics to modify the ISMC such that cross-coupling is achieved. Define the following modified error variables

$$\tilde{p}_i = \tilde{p}_i + \gamma \epsilon_i \quad (15)$$

$$\tilde{v}_i = \tilde{v}_i + \gamma \frac{d}{dt} \epsilon_i, \quad (16)$$

where  $\gamma$  is a positive constant. A trade-off between position tracking and contouring can be achieved by proper selection of  $\gamma$ . In other words,  $\gamma = 0$  results in no cross-coupling and large  $\gamma$  means low-performance position tracking. Using  $\tilde{p}$  and  $\tilde{v}$  and system equations (1) and (2) gives

$$\frac{d}{dt} \tilde{p}_i = \tilde{v}_i \quad (17)$$

$$\frac{d}{dt} \tilde{v}_i = -\frac{1}{\tau_i} \tilde{v}_i - \frac{k_i}{\tau_i} u_i + \frac{d^2}{dt^2} r_i + \frac{1}{\tau_i} \frac{d}{dt} r_i - \frac{k_i}{\tau_i} \tilde{d}_i, \quad (18)$$

where

$$\tilde{d}_i = d_i - \frac{\gamma}{k_i} \left( \tau_i \frac{d^2}{dt^2} \epsilon_i + \frac{d}{dt} \epsilon_i \right), \quad \left| \tau_i \frac{d^2}{dt^2} \epsilon_i + \frac{d}{dt} \epsilon_i \right| \leq N_i, \quad (19)$$

which augments the first and second order derivatives of the CEE in disturbance to avoid noise amplification during control design and implementation. One can then design ISMC based on (17) and (18) using the equivalent control design method, the result of which is summarized in the following theorem.

*Theorem 1:* Assume a multi-axis servosystem is given as (1) and (2), and the disturbances acting on the system are upper-bounded as  $|d_i| \leq M_i$ , where  $M_i$  is a positive real number. Moreover, the reference inputs,  $r_i(\theta)$ , and their first time derivatives,  $dr_i(\theta)/dt$ , are smooth and differentiable. Assume an estimate of contour error is available such that  $|\tau_i d^2 \epsilon_i / dt^2 + d \epsilon_i / dt| \leq N_i$ , where  $N_i$  is a positive real number. Control signals of the form:

$$u_i^{\text{ismc}} = \left( \frac{(a_i + b_i) \tau_i - 1}{k_i} \right) \tilde{v}_i + \left( \frac{a_i b_i \tau_i}{k_i} \right) \tilde{p}_i + \frac{\tau_i}{k_i} \frac{d^2}{dt^2} r_i + \frac{1}{k_i} \frac{d}{dt} r_i + \kappa_i \mu_i \text{sat} \left( \frac{\sigma_i}{\mu_i} \right), \quad (20)$$

govern the system asymptotically to the desired reference positions for positive real numbers  $a_i, b_i, \mu_i$ , and  $\gamma$ , and the switch parameter satisfying

$$\kappa_i \geq \frac{k_i M_i + \gamma N_i}{\mu_i k_i} + \frac{b_i \tau_i}{k_i}. \quad (21)$$

The switching equation is given as

$$\sigma_i = \tilde{v}_i + a_i \tilde{p}_i + b_i q_i, \quad (22)$$

where

$$\frac{d}{dt} q_i = -b_i q_i + \mu_i \text{sat} \left( \frac{\sigma_i}{\mu_i} \right), \quad (23)$$

where  $\text{sat}(x) = x$  for  $|x| \leq 1$  and  $\text{sat}(x) = \text{sign}(x)$  for  $|x| > 1$ . ■

*Proof:* An outline of the proof is presented. Define a Lyapunov function as  $W_i = \sigma_i^2 / 2$ . Using control signal (20) and the condition (21) one can easily show that  $dW_i/dt$  is negative definite which proves that the sliding surface is stable. Then, using linearization for  $|\sigma_i| \leq \mu_i$  one can show that the equilibrium is asymptotically stable. ■



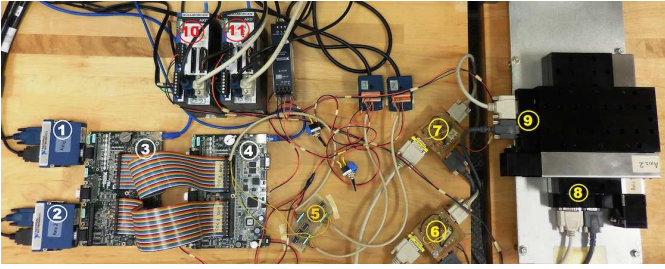


Fig. 6. Experimental setup (1 and 2) NI 9514, (3) sbRIO for position control, (4) sbRIO for CEE and/or CCC, (5) RS-485 to TTL adapter, (6 and 7) Hall sensors and incremental encoder adapter, (8) Axis-1, (9) Axis-2, and (10 and 11) AKD servo-drives

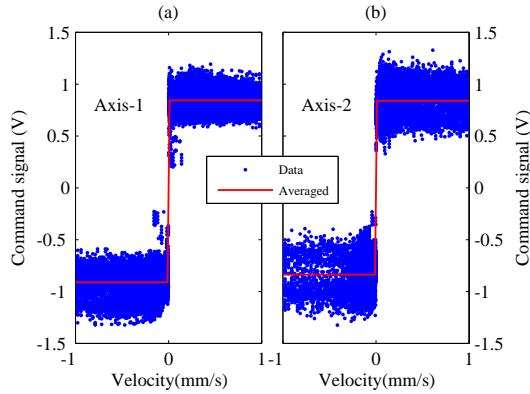


Fig. 7. Friction characteristic (a) Axis-1 and (b) Axis-2

The control loop sampling rate is  $\tau_s = 0.1$  ms. The single boards and servo-drives are connected to the host computer through an ethernet hub. Reference contour interpolation and data acquisition is a part of the host program. A picture of the experimental setup is shown in Fig. 6.

According to (21), one should know disturbance upper bound,  $M_i$ , to design the switch gain,  $\kappa_i$ . In the proposed experiment setup, disturbance is dominated by friction. Also, viscosity can be modeled fairly accurate as a linear term proportional to axis velocity and be included in the system dynamic equations. On the other hand, stiction is discontinuous and considerably larger than viscosity. Hence, the presented friction test on the experimental setup is conducted to identify stiction, the results of which are shown in Fig. 7. The collected data confirms that both axes have almost identical stiction characteristic with slightly larger level for negative speeds on Axis-1. The combined stiction and Coulomb averaged models are given as

$$f_1^c = \begin{cases} 0.84, & v_1 > 0 \text{ or } u_1 > 0.84 \\ u_1, & v_1 = 0 \text{ or } -0.91 \leq u_1 \leq 0.84 \\ -0.91, & v_1 < 0 \text{ or } u_1 < -0.91 \end{cases} \quad (28)$$

$$f_2^c = \begin{cases} 0.84 \operatorname{sign}(u_2), & v_2 \neq 0 \text{ or } |u_2| > 0.84 \\ u_2, & v_2 = 0 \text{ or } |u_2| \leq 0.84 \end{cases} \quad (29)$$

The data is collected for  $-30 \text{ mm} \leq p_i \leq 30 \text{ mm}$  with five different measurements for each point.

Unlike conventional feedforward friction compensation algorithms that rely heavily on friction model and system identi-

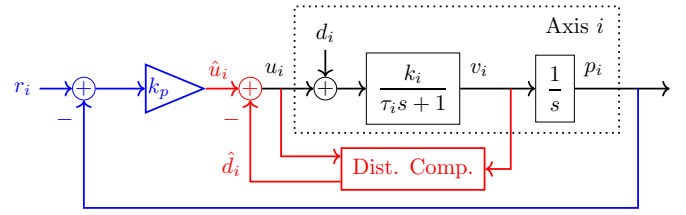


Fig. 8. Closed-loop configuration for system identification of axis  $i$

fication, adaptive disturbance estimation (25) does not require further identification and tuning to account for the effects of temperature and aging. The friction test is only conducted to roughly estimate the disturbance upper bound,  $M_i$ , which will be further reduced after disturbance compensation. In other words, the friction identification gives a conservative estimate of  $M_i$ .

For simplicity it is assumed that the servo-drive and its current control loop is a part of each axis model. Hence, the identified model shows the relationship between position in mm and the drive command which varies between  $\pm 10$  V. Thus, after initial open loop identification, a proportional controller,  $k_p = 1$ , is designed for each axis. A closed-loop configuration for system identification of each axis is shown in Fig. 8. Initialization of parameters  $k_i$  and  $\tau_i$  is required to conduct the identification experiment. The disturbance compensation adaptively estimates  $d_i$  which is dominated by friction,  $f_i^c$ . However, due to parametric uncertainty and other sources of disturbance,  $d_i$  does not arise only due to friction. A sufficiently accurate estimate of system parameters results in  $\hat{d}_i \approx d_i$ . Thus, one can disregard the effect of disturbance in the closed-loop system. The time domain reference signal,  $r_i$ , and position measurement,  $p_i$ , are used for system identification. Given  $k_p = 1$ , the closed-loop transfer function is

$$\frac{p_i}{r_i} = \frac{k_i/\tau_i}{s^2 + s/\tau_i + k_i/\tau_i}. \quad (30)$$

The System Identification toolbox of MATLAB is used to estimate the second order closed-loop transfer function (30). Since the disturbance compensation depends on nominal system dynamics and requires initialization, one can update the control loop after model identification and repeat the experiment to obtain a more precise estimate of  $k_i$  and  $\tau_i$ .

Disturbance compensation (25) is initially designed based on the open-loop system identification and then updated based on the closed-loop system identification. After multiple iterations the closed-loop identification gives the overall system dynamics, for Axis-1 and Axis-2 respectively, as

$$G_1(s) = \frac{28.2}{s(0.11s + 1)} \quad (31)$$

$$G_2(s) = \frac{41.8}{s(0.17s + 1)}, \quad (32)$$

where the transfer function fit to estimation is excellent, (i.e., 96.36% for  $G_1(s)$  and 95.09% for  $G_2(s)$ ), which verifies the effectiveness of the adaptive disturbance compensation. The nominal state space model of each axis, equations (1) and (2) with  $d_i = 0$ , is obtained from identified transfer functions (31)

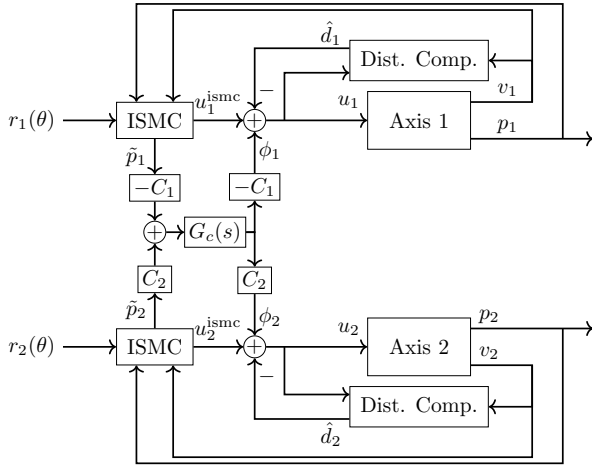


Fig. 9. Integrated CCC of a two-axis servosystem using ISMC [1], [22], [29] and static CEE [15], [33], [35]

and (32). The nominal model is then used to design the ISMC and disturbance compensation algorithm.

*Remark 5:* The servo-drive receives a drive command from a NI 9514 drive interface module with 16 bits of resolution. The incremental encoder generates 8,000 counts per mm. Thus, DAC-encoder interface introduces a loop gain of 0.41 to the experiment setup which needs to be compensated when the control is implemented.

Using the obtained models the ISMC is designed, where  $a_i = b_i = 20, c_i = 50, w_i = \omega = 3000 \text{ rad/s}, \kappa_i = 4$ , and  $\mu_i = 0.125$ . In the next section various experiments are conducted to verify the effectiveness of the Newton-based CEE and modified ISMC for cross-coupling for different contours. The results of our proposed algorithm, shown in Fig. 4, are compared with the contouring algorithm shown in Fig. 9, where  $G_c(s) = 5 + 0.5s$  and the ISMC parameters are the same as those given for the modified ISMC. Different variations of contouring algorithm in Fig. 9 with [22] and without [1], [29] static contour error estimation [15], [33], [35] have been studied by other researchers. The conventional ISMC design used in Fig. 9 operates on axis errors  $\tilde{p}_i$  and  $\tilde{v}_i$  while the modified ISMC operates on modified errors  $\check{p}_i$  and  $\check{v}_i$ .

## V. EXPERIMENTAL RESULTS

Feedrate,  $\varphi_c$ , is an important factor in contouring and equals the contour linear velocity in mm/s, which for a circular contour is defined as

$$\varphi_c = \omega_c r_c, \quad (33)$$

where  $\omega_c$  is angular velocity in rad/s and  $r_c$  is the circle radius in mm.

The dynamic CEE was first verified using numerical simulations with linear models similar to (31) and (32) and a Coulomb friction model [10]. However, in reality the system dynamics are more complicated with highly nonlinear terms. Also, the linear model is valid in a small neighborhood around the working point. More realistic system dynamics are needed to evaluate the performance of the proposed algorithm

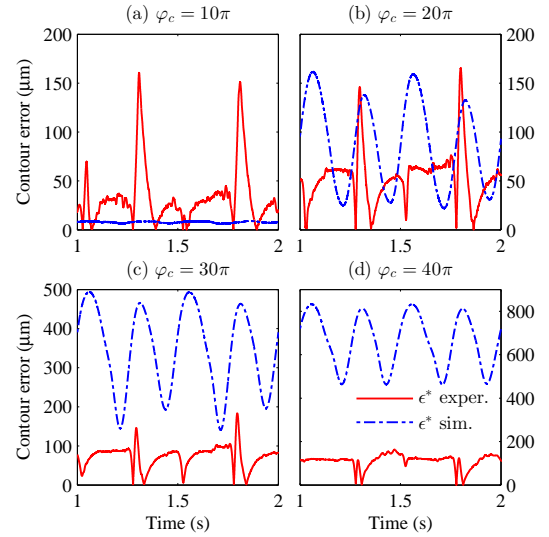


Fig. 10. Comparison between numerical simulation and experimental results with feedrate (a)  $10\pi$ , (b)  $20\pi$ , (c)  $30\pi$ , and (d)  $40\pi$  mm/s and  $\omega_c = 2\pi$  rad/s

using numerical simulation. A comparison between numerical simulation and experimental results is presented for different feedrates. The same control algorithms with the same level of numerical precision are used in both cases. The simulations are conducted using linear models (31) and (32). Regardless of the reference contour feedrate, the numerical simulation stays far from experimental results, as shown in Fig. 10. Hence, numerical simulation based on simplified model dynamics cannot be used for performance verification. Moreover, the position control is designed with robustness objectives in mind to avoid high order system identification and to eliminate the effect of external disturbances. Thus, this section focuses on experimental results.

The preliminary experiments were carried out with 6 different reference contours to show the effectiveness of the dynamic CEE in contouring [9]. The presented experiments in this paper include 13 different reference contours with the proposed algorithm tuned to achieve the best possible contouring. The experiments are conducted as follows: 1) the Newton-based CEE performance and its improvement over the static CEE is studied, 2) the modified feedback design is analyzed with contour maps with different feedrates, and 3) the proposed contouring algorithm is tested for sharp corners. In the first two steps circular contours with different feedrate and radius are used while in the third step an astroid reference contour (see Fig. 15) is used to perform the experiments.

### A. Performance of the Newton-Based CEE

A circular contour with  $r_c = 10$  mm and  $\varphi_c = 10\pi$  mm/s is used. The contour error is not present in the position control, i.e.,  $\gamma = 0$ . The number of iterations are changed and the CEE is compared with the actual contour error. Two criteria are introduced to compare the effect of iteration number on the CEE performance:

$$\delta_{\max} = \max_{1 \leq j \leq N_t} \delta(j\tau_s) \quad (34)$$

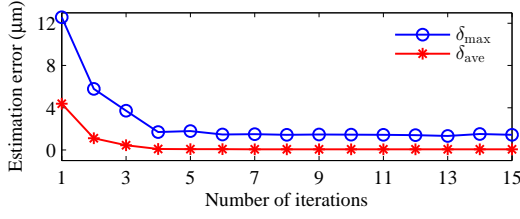
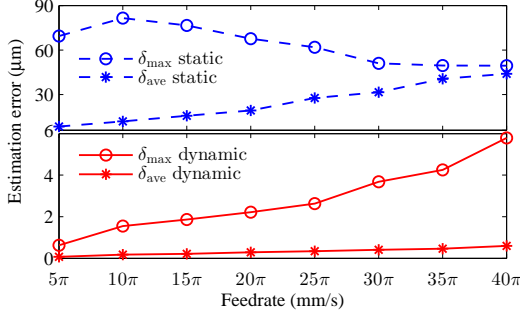


Fig. 11. Effect of number of iterations on the Newton-based CEE precision

Fig. 12. Comparison between static and dynamic CEE for reference set  $R_\pi$ 

$$\delta_{\text{ave}} = \frac{1}{N_t} \sum_{j=1}^{N_t} \delta(j\tau_s), \quad (35)$$

where  $\delta(j\tau_s) = \|\epsilon(j\tau_s)\| - \|\epsilon^*(j\tau_s)\|$  is absolute estimation error, where  $\epsilon^*(j\tau_s)$  is the actual contour error and  $\epsilon(j\tau_s)$  is the contour estimate from CEE algorithm. Total number of time steps is  $N_t$ . As shown in Fig. 11, after five iterations the averaged value of the estimation error is very close to zero. However, the maximum value can be slightly reduced by increasing the number of iterations to ten. Iterations more than ten have little effect on reducing the average or maximum value. Hence, from this point forward the number of iterations for the dynamic CEE is fixed at ten.

Consider a set of reference contours as

$$R_\pi = \{(\omega_c = \pi, \varphi_c = 5K\pi), K = 1, 2, \dots, 8\}. \quad (36)$$

The contour error gain is set to  $\gamma = 20$  to achieve cross-coupling. The performance of the dynamic CEE versus the static CEE for  $R_\pi$  is shown in Fig. 12. The dynamic estimate reduces  $\delta_{\text{max}}$  and  $\delta_{\text{ave}}$  by an average factor of 37 and 81, respectively, in comparison to the static algorithm.

### B. Contours with Different Feedrates and Curvatures

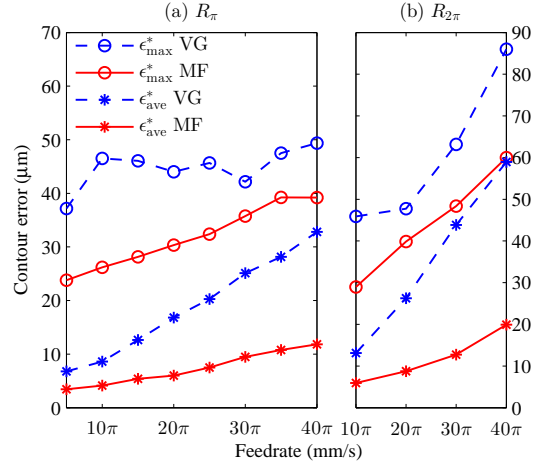
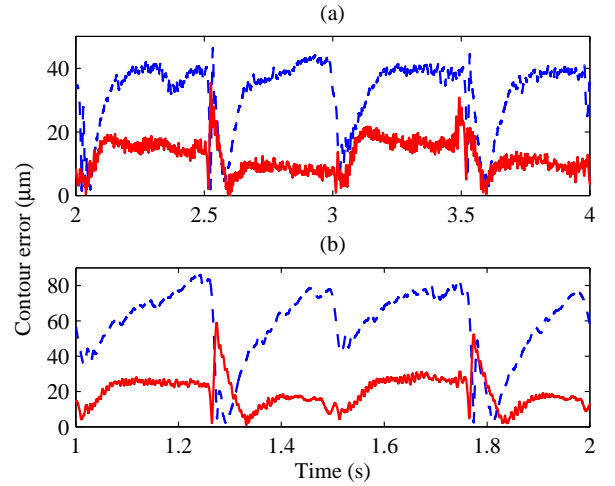
Maximum and averaged contour errors are defined as follows

$$\epsilon_{\text{max}}^* = \max_{1 \leq j \leq N_t} \{\|\epsilon^*(j\tau_s)\|\} \quad (37)$$

$$\epsilon_{\text{ave}}^* = \frac{1}{N_t} \sum_{j=1}^{N_t} (\|\epsilon^*(j\tau_s)\|). \quad (38)$$

Another set of reference contours with higher angular speed is defined as

$$R_{2\pi} = \{(\omega_c = 2\pi, \varphi_c = 10K\pi), K = 1, 2, 3, 4\}. \quad (39)$$

Fig. 13. Variation of  $\epsilon_{\text{max}}^*$  and  $\epsilon_{\text{ave}}^*$  for reference set (a)  $R_\pi$  and (b)  $R_{2\pi}$ Fig. 14. Variation of contour error for (solid red) the proposed scheme, and (dashed blue) variable gain algorithms, where  $\varphi_c = 40\pi$  mm/s and (a)  $\omega_c = \pi$  rad/s and (b)  $\omega_c = 2\pi$  rad/s

A comparison between contouring performance of the proposed modified feedback (MF) scheme and the variable gain (VG) algorithm for  $R_\pi$  and  $R_{2\pi}$  is shown in Fig. 13. The proposed algorithm reduces  $\epsilon_{\text{max}}^*$  and  $\epsilon_{\text{ave}}^*$  by average percentages of 29 and 60, respectively, for  $R_\pi$  in comparison to the variable gain algorithm. The proposed algorithm reduces  $\epsilon_{\text{max}}^*$  and  $\epsilon_{\text{ave}}^*$  by average percentages of 27 and 65, respectively, for  $R_{2\pi}$  in comparison to the variable gain algorithm. A plot of contour error evolution versus time for the proposed algorithm and variable gain CCC is shown in Fig. 14 with  $\varphi_c = 40\pi$  mm/s and  $\omega_c = \pi$  rad/s at the top plot and  $\omega_c = 2\pi$  rad/s at the bottom plot. In both experiments the proposed modified feedback design performs better than the variable gain CCC.

### C. Sharp Corners

An astroid reference contour, as shown in Fig. 15, is used to verify the effectiveness of the proposed algorithm for contours with sharp corners. The contour completes one turn in 2 s and the maximum feedrate is  $60\pi$  mm/s. As shown in

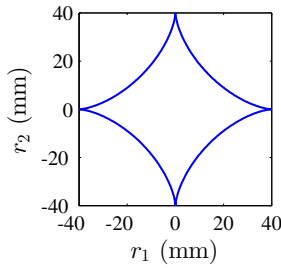


Fig. 15. Astroid reference contour

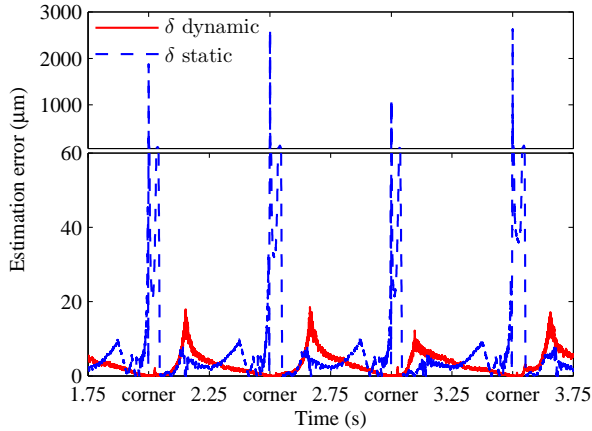


Fig. 16. Absolute estimation error for astroid reference map for (solid red) dynamic and (dashed blue) static CEE algorithms

Fig. 16, while the absolute estimation error,  $\delta$ , of the Newton-based CEE stays less than  $20 \mu\text{m}$ , the static CEE design has considerably larger estimation error at the corners. However, one may notice that the Newton CEE, in several points between the corners, does not perform as precise as the static CEE. There are two reasons behind this phenomenon: 1) the feedrate increases as the contour lead point moves away from the corners which reduces the accuracy of the Newton CEE. After a transient, the accurate estimate is restored; and 2) the reference map between the corners acts in favor of the static CEE since it can be approximated precisely as a second order curve which results in accurate static contour error estimate. There is a performance trade-off between deep corners and low order curves. The proposed algorithm highly improves the performance around deep corners and is sufficiently accurate elsewhere. However, the variable gain algorithm is highly unreliable around deep corners and accurate for low order curves. As shown in Fig. 17, the proposed algorithm tracks corners more precisely than the variable gain algorithm.

## VI. CONCLUSIONS

The experiments conducted demonstrate that the proposed dynamic CEE achieves almost the exact estimate of actual contour error regardless of reference feedrate and curvature. Instead of designing a separate control for cross-coupling, the concept of feedback modification is proposed to alleviate the need for designing a separate CCC. Thus, ISMC control, designed for each axis, is modified such that the effect of

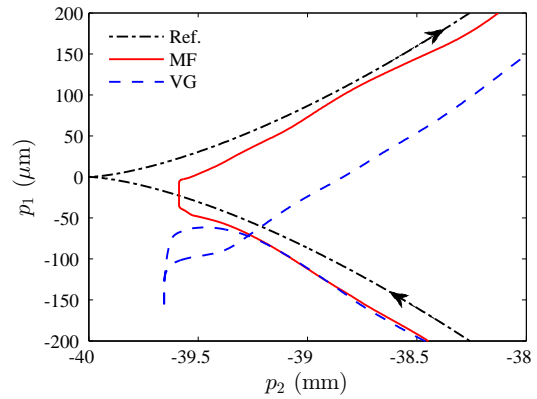


Fig. 17. Contouring performance of the proposed algorithms versus the variable gain design

contour error is incorporated in the position control algorithm. The theoretical analysis showed that the the modified ISMC design results in perfect tracking and zero contour error. Our proposed design results in a high-performance CEE, better contouring precision, and less design steps. In comparison to the variable gain CCC class of methods, the proposed design reduces contouring error by a factor of two. Moreover, sharp corners are also tracked more precisely.

Future research should consider an industrial scale stage in commercial machines which may perform quite differently compared to a laboratory scale two-axis stage from several perspectives such as friction effects, inertial effects, and vibration.

## REFERENCES

- [1] Y. Altintas, K. Erkorkmaz, and W.-H. Zhu, "Sliding mode controller design for high speed feed drives," *CIRP Annals - Manufacturing Technology*, vol. 49, pp. 265–270, 2000.
- [2] B. Chen, D. Tilbury, and A. Ulsoy, "Modular control for machine tools: Cross-coupling control with friction compensation," in *Proc. of ASME IMECE*, 1998.
- [3] C.-S. Chen and L.-Y. Chen, "Cross-coupling position command shaping control in a multi-axis motion system," *Mechatronics*, vol. 21, pp. 625–632, 2011.
- [4] S.-L. Chen and K.-C. Wu, "Contouring control of smooth paths for multi-axis motion systems based on equivalent errors," *IEEE Transactions on Control System Technology*, vol. 15, pp. 1151–1158, 2007.
- [5] M.-Y. Cheng, K.-H. Su, and S.-F. Wang, "Contour error reduction for free-form contour following tasks of biaxial motion control systems," *Robotics and Computer-Integrated Manufacturing*, vol. 25, pp. 323–333, 2009.
- [6] M.-Y. Cheng and C.-C. Lee, "Motion controller design for contour-following tasks based on real-time contour error estimation," *IEEE Transactions on Industrial Electronics*, vol. 54, pp. 1686–1695, 2007.
- [7] H.-Y. Chuang and C.-H. Liu, "Cross-coupled adaptive feedrate control for multi-axis machine tools," *Journal of Dynamic Systems, Measurement, and Control*, vol. 113, pp. 451–457, 1991.
- [8] K. Fujimoto, K. Sakurama, and T. Sugie, "Trajectory tracking control of port-controlled Hamiltonian systems via generalized canonical transformations," *Automatica*, vol. 39, pp. 2059–2069, 2003.
- [9] A. Ghaffari and A. G. Ulsoy, "Experimental verification of dynamic contour error estimation for high-precision contouring of two-axis servosystems," in *Proc. of ASME Dynamic Systems and Control Conference*, 2015.
- [10] —, "Newton-based contour error estimation and robust cross-coupling control for high-precision fast contouring," in *Proc. of American Control Conference*, 2015.
- [11] A. Ghaffari, M. Krstić, and D. Nešić, "Multivariable Newton-based extremum seeking," *Automatica*, vol. 48, pp. 1759–1767, 2012.

- [12] C. Hu, B. Yao, and Q. Wang, "Coordinated adaptive robust contouring controller design for an industrial biaxial precision gantry," *IEEE/ASME Transactions on Mechatronics*, vol. 15, pp. 728–735, 2010.
- [13] F. Huo and A.-N. Poo, "Improving contouring accuracy by using generalized cross-coupled control," *International Journal of Machine Tools & Manufacture*, vol. 63, pp. 49–57, 2012.
- [14] O. Khatib, "A unified approach for motion and force control of robot manipulators: The operational space formulation," *IEEE Journal of Robotics and Automation*, vol. RA-3, pp. 43–53, 1987.
- [15] Y. Koren and C.-C. Lo, "Variable-gain cross-coupling controller for contouring," *CIRP Annals - Manufacturing Technology*, vol. 40, pp. 371–374, 1991.
- [16] Y. Koren, "Cross-coupled biaxial computer control for manufacturing systems," *Journal of Dynamic Systems, Measurement, and Control*, vol. 102, pp. 265–272, 1980.
- [17] D. Lam, C. Manzie, and M. C. Good, "Model predictive contouring control for biaxial systems," *IEEE Transactions on Control System Technology*, vol. 21, pp. 552–559, 2013.
- [18] F.-J. Lin, P.-H. Chou, C.-S. Chen, and Y.-S. Lin, "DSP-based cross-coupled synchronous control for dual linear motors via intelligent complementary sliding mode control," *IEEE Transactions on Industrial Electronics*, vol. 59, pp. 1061–1073, 2012.
- [19] C.-C. Lo, "An improved algorithm for cross-coupling control of multi-axis machine tools," *Journal of Manufacturing Science and Engineering*, vol. 121, pp. 537–540, 1999.
- [20] C.-C. Lo and C.-Y. Chung, "Tangential-contouring controller for biaxial motion control," *Journal of Dynamic Systems, Measurement, and Control*, vol. 121, pp. 126–129, 1999.
- [21] W. H. Moase, C. Manzie, and M. J. Brear, "Newton-like extremum-seeking for the control of thermoacoustic instability," *IEEE Transactions on Automatic Control*, vol. 55, pp. 2094–2105, 2010.
- [22] A. Mohammad A. M., N. Uchiyama, and S. Sano, "Energy saving in feed drive systems using sliding-mode-based contouring control with a nonlinear sliding surface," *IEEE/ASME Transactions on Mechatronics*, vol. 20, pp. 572–579, 2015.
- [23] M. Rahaman, R. Seethaler, and I. Yellowley, "A new approach to contour error control in high speed machining," *International Journal of Machine Tools & Manufacture*, vol. 88, pp. 42–50, 2015.
- [24] K. Srinivasan and P. K. Kulkarni, "Cross-coupled control of biaxial feed drive servomechanisms," *Journal of Dynamic Systems, Measurement, and Control*, vol. 112, pp. 225–232, 1990.
- [25] K.-H. Su, H.-R. Chen, and M.-Y. Cheng, "Free-form curves contour error estimation using the backward arc length approach," in *Proc. of 2014 IEEE/SICE International Symposium on System Integration*, 2014.
- [26] D. Sun, "Position synchronization of multiple motion axes with adaptive coupling control," *Automatica*, vol. 39, pp. 997–1005, 2003.
- [27] L. Tang and R. G. Landers, "Predictive contour control with adaptive feed rate," *IEEE/ASME Transactions on Mechatronics*, vol. 17, pp. 669–679, 2012.
- [28] —, "Multiaxis contour control—the state of the art," *IEEE Transactions on Control System Technology*, vol. 21, pp. 552–559, 2013.
- [29] X.-C. Xi, G.-S. Hong, and A.-N. Poo, "Improving CNC contouring accuracy by integral sliding mode control," *Mechatronics*, vol. 20, pp. 442–452, 2010.
- [30] Y. Xiao, K. Zhu, and H. Liaw, "Generalized synchronization control of multi-axis motion systems," *Control Engineering Practice*, vol. 13, pp. 809–819, 2005.
- [31] J. Yang and Z. Li, "A novel contour error estimation for position loop-based cross-coupled control," *IEEE/ASME Transactions on Mechatronics*, vol. 16, pp. 643–655, 2011.
- [32] B. Yao, C. Hu, and Q. Wang, "An orthogonal global task coordinate frame for contouring control of biaxial systems," *IEEE/ASME Transactions on Mechatronics*, vol. 17, pp. 622–634, 2012.
- [33] S.-S. Yeh and P.-L. Hsu, "Estimation of the contouring error vector for the cross-coupled control design," *IEEE/ASME Transactions on Mechatronics*, vol. 7, pp. 44–51, 2002.
- [34] Z.-M. Yeh, Y. Trang, and Y. Lin, "Cross-coupled fuzzy logic control for multiaxis machine tools," *Mechatronics*, vol. 7, pp. 663–681, 1997.
- [35] L. Zhu, H. Zhao, and H. Ding, "Real-time contouring error estimation for multi-axis motion systems using the second-order approximation," *International Journal of Machine Tools & Manufacture*, vol. 68, pp. 75–80, 2013.



**Azad Ghaffari** is a Postdoctoral Research Fellow in the Mechanical Engineering Department at University of Michigan, Ann Arbor. He received the B.S. degree in electrical engineering and the M.S. degree in control engineering from the K. N. Toosi University of Technology, Tehran, Iran, and the Ph.D. degree in mechanical and aerospace engineering from the Joint Doctoral Program between San Diego State University and the University of California, San Diego, CA, USA. His current research interests include distributed supervisory controller design for swapping modularity, cross-coupling control of multi-axis servo-systems, demand response in power systems, extremum seeking and its application to maximum power point tracking in photovoltaic and wind energy conversion systems, induction machines, power electronics, and sliding mode control.



**A. Galip Ulsoy** is C.D. Mote, Jr. Distinguished University Professor of Mechanical Engineering and W.C. Ford Professor of Manufacturing at University of Michigan, Ann Arbor. He received the Ph.D. from University of California at Berkeley (1979), M.S. from Cornell University (1975), and B.S. from Swarthmore College (1973). His research interests are in dynamics and control of mechanical systems. He has received numerous awards, including the 2008 Rufus T. Oldenburger Medal and the 2013 Charles Russ Richards Award from ASME, is a member of the National Academy of Engineering and is a Fellow of ASME, SME, IEEE and IFAC.